Towards echocardiographic strain imaging of the mitral valve leaflets using block matching approaches

Ana Lúcia Grilo Martins de Brito Barriga
ana.barriga@tecnico.ulisboa.pt

Instituto Superior Técnico, Lisboa, Portugal

September 2020

Abstract

Mitral regurgitation, namely secondary mitral regurgitation, is the second most prevalent type of valvular heart disease worldwide. Quantitative two-dimensional (2D) echocardiography has become the most suitable imaging modality for diagnosing such diseases. Nevertheless, due to its particularities in evaluation and quantification, further improvements in current echocardiographic equipment are needed to ensure a more accurate assessment of valvular function.

The goal of this study was to investigate the performance of currently emerging techniques in this field, namely 2D speckle tracking techniques, in understanding and quantifying mitral valve leaflets' kinematics and strains throughout the cardiac cycle, spotting their main advantages and limitations.

Several motion tracking techniques based on standard and more robust optimization-based block matching algorithms, commonly used when performing speckle tracking, were implemented. Besides, a framework for the generation of synthetic images was developed in order to allow the validation and assessment of the proposed methods.

When examining each algorithm's performance carefully using the generated synthetic images, the results show that an optimization-based block matching approach was the most suited for addressing complex motion patterns, as the bending-like behaviour of the mitral leaflets during the key-events of the cardiac cycle. However, the deformation estimates returned by this algorithm are highly dependent on the resolution of the displacement field obtained, therefore providing only qualitative information. When analysing real echocardiographic images, such findings are corroborated, emphasizing the difficulties of the algorithm in capturing wider displacements of the leaflets and its dependence on the image quality and the number of frames analysed.

Keywords: Mitral valve, deformation imaging, speckle tracking, block matching, echocardiography.

1. Introduction

Data from the Euro Heart Survey [10] show that mitral regurgitation (MR) is the second most frequent valvular heart disease (VHD) worldwide. It consists of a leaky mitral valve allowing blood to flow backwards into the left atrium. It can be either due to primary anatomical deformities of the mitral leaflets and chordae or to functional impairments and enlargement of the left ventricle and mitral apparatus. In the latter case, it is named secondary MR (SMR), being present in approximately 50% of patients after myocardial infarction and always worsening their prognosis [10]. The disease's main mechanism is tethering of the mitral leaflets because of papillary muscles' displacement and reduced closing forces associated with regional and global contractility and dyssynchrony of the left ventricle [7].

However, it remains difficult to assess the anomalies that lead to the disease because of its particularities in classification and quantification [7]. Symptoms are subjective and only detailed echocardiographic examination can reliably differentiate SMR from other types of MR, helping to establish its aetiology and mechanisms, to quantify its severity, progression and consequences, and to determine the best treatment through the acquisition of specific measurements of the mitral valve apparatus [12]. Preliminary evidence indicates that novel echocardiographic quantities such as strain and strain rate may provide valuable prognostic information [7, 4].

Deformation echocardiography has become widely used in the clinical practice due to its low costs, accessibility, non-invasiveness and intrinsic dynamic nature, ideally suited for the evaluation of cardiac mechanics and deformation [1]. It can be performed through the speckle tracking echocardiography (STE) technique. It is based on tracking characteristic speckle patterns created by interference of ultrasound beams in the cardiac tissues frame by frame. Local displacement

information is obtained, from which parameters regarding tissue velocity, strain or strain rate can be derived [8].

Clinical feasibility and reliability of strain derived from STE have been shown in many studies. Its main application is the assessment of left ventricular function [8]. Analogous information regarding motion and strains can be useful in spotting some of the pathophysiologic differences and establishing objective parameters that diagnose SMR. If it is possible to quantify different levels of SMR, or better evaluate the functional limitations of the valve, better therapy can be delivered to the patient [7].

Over the last 20 years, several clinical software algorithms and tools for STE have been marketed by different vendors. They rely on already existing methodologies used for motion tracking, based on optical flow and image registration approaches. Among them, block matching (BM) methods, which became popular due to their robustness, simplicity and versatility, are preferred [8].

Despite being computationally efficient, they are vulnerable to the presence of noise and texture and brightness changes, commonly found in ultrasound images [14]. Besides, the motion vectors (MVs) must be related to each other so that a realistic motion field is estimated. Therefore, various methodologies to improve BM have arisen, in which the aim is to introduce a smoothing or regularization aspect to the initial estimates of the MVs. On the one hand, a weighted smoothing of neighbouring MVs estimates can be done [6]. On the other hand, optimization-based BM processes that integrate physiological constraints of smoothness of the displacements' field into the tracking algorithm can be introduced to overcome the limitation of speckle decorrelation noise [11, 3].

Considering the success of 2D STE for myocardial analysis, this work aimed to investigate the application of similar techniques for the evaluation and estimation of the mitral valve leaflets kinematics, including their motion and strains, throughout the cardiac cycle. A qualitative and quantitative evaluation of these standard BM algorithms was ascertained using synthetic images, and their advantages and limitations established while understanding the main challenges of studying the mitral valve motion through a real echocardiographic sequence.

2. Methods

2.1. *Full search* algorithm

The idea behind BM is to define a set of blocks (kernels) in a current frame k and then compare them with the corresponding blocks and adjacent neighbours in a reference frame *k+1* to create motion vectors (MVs) that represent the motion of each block from one frame to another. For a given block, its MV is computed by finding the best suitable block matched according to a similarity criterion [14].

A given block of interest is searched for within a search window. In the case of the *full search* algorithm, the search window corresponded to a square centred on the block of interest, defined on the reference image, whose width is specified by p.

The best match between two blocks was established with the use of the sum of absolute differences (SAD) as cost function. It is the simplest possible metric that takes into account every pixel in a block, being very effective for a wide motion search of many different blocks [8, 14]. For a block area of $n \times n$, the SAD is expressed as:

$$SAD = \sum_{i=0}^{n-1} \sum_{j=0}^{n-1} |C_{ij} - R_{ij}| \tag{1}$$

where C_{ij} and R_{ij} are samples from the current and reference frames, respectively.

The search window was fully scanned, and the value of the cost function at each possible position within it was computed, assuring that the best MV was found. Note that each block was processed independently.

2.2. Rotational BM

The *full search* algorithm can be modified so that it combines both translational and rotational motions, common in image sequences. To implement rotation, a transformation of coordinates must be performed in the reference frame to obtain rotated versions of the reference block [13]. The coordinates of the sub-sampled pixels positions are given by:

$$x_2 = \cos\theta(x_1 - x_0) + \sin\theta(y_1 - y_0) + x_0 \tag{2}$$

$$y_2 = \cos\theta(y_1 - y_0) - \sin\theta(x_1 - x_0) + y_0 \tag{3}$$

where θ is the rotation angle, x_0 and y_0 are the coordinates of the centre of rotation, x_1 and y_1 are the original coordinates, and finally x_2 and y_2 are the rotated coordinates, all of them reported in the reference frame. For each block, the centre of rotation was defined at its centroid.

After that, interpolation is again required to obtain the intensity values of these sub-sampled pixels positions. Whenever there is a rotated block, the SAD is computed between the current and the reference block using these intermediate intensities. The MV associated with the position and rotation angle that have the lowest SAD is returned.

The proposed rotation strategy consists in applying the *full search* algorithm using traditional integer motion tracking and performing rotation at each position. To fix the number of BM operations between these, a search angle interval and a search angle range were defined.

2.3. Neighbourhood averaging

The pixels of the same moving object are expected to move consistently. If the global motion trend of an entire neighbourhood is considered, MVs can be more accurately estimated, and tracking issues due to noise or complex motions are better handled [6].

The basics underlying the proposed approach are presented in Figure 1. To incorporate neighbouring information, a weighting strategy must be defined. Different weighting factors are assigned to neighbouring blocks according to a distance criterion defined by two parameters: d, which corresponds to the distance between the central block and one of its neighbours, and D, the radius of a circumference centred on the central block, both in pixels. The weighting factors are given by:

$$w = \max\{0, D - d\} \tag{4}$$

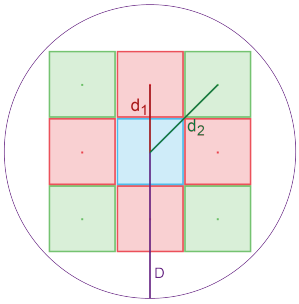

Figure 1: Neighbourhood averaging strategy: the central block of interest is represented in blue, while the four closest neighbours are represented in red and the remaining four in green. Parameter d is depicted as d_1 and d_2, respectively for the *type* 1 and *type* 2 neighbours.

After obtaining the first MVs estimates for all blocks from the *full search* algorithm between two consecutive frames k and $k+1$, a linear weighted averaging was then performed using the corresponding weighting factors to obtain the final MVs estimates, which can consider either the 4 nearest (*type*=1) or the total 8 (*type*=2) neighbouring blocks.

The weights are seen to decay linearly with the distance. Note that parameter D delimits the filter area and regulates the importance of the neighbourhood averaging. If all pixels within a given neighbouring block have intensities below 50, a criterion that is based on the characteristics of echocardiographic images with a pixel depth of 8 bit, the block is disregarded in the weighted average as it is considered not to have relevant information.

2.4. Optimization-based BM algorithm

In order to be more robust to speckle decorrelation noise, the tracking can be formulated as an optimization problem that jointly penalizes intensity disparity and motion discontinuity [11, 3]. The proposed method combines the BM algorithm with a smoothness constraint for a neighbourhood of blocks ϕ, and minimizes a cost function f in which the design variables $\mathbf{b}$ corresponds to the MVs of all blocks in ϕ, between frames k and $k+1$. Mathematically, the optimization problem is expressed as:

$$f = \sum_{\phi}(E_S + \lambda E_R) \tag{5}$$

$$\underset{\mathbf{b}}{\text{minimize}} \quad f(\mathbf{b}) \tag{6}$$

The first term E_S is the total penalty for speckle decorrelation and dissimilarity between images, measured by the sum of the SADs for all the blocks. The second term E_R penalizes the loss of displacement continuity and smoothness, thus acting as a regularization term. The parameter λ weights the regularization term versus the data matching term.

2.4.1 Regularization function

The regularization function was chosen to be the strain energy (SE), corresponding to the energy stored by a system undergoing deformation. A FE code is implemented to obtain the SE for a given configuration [5]. To simplify the problem, it was assumed that the body was an isotropic linear elastic solid, there were null body forces, and there was a plane strain deformation state.

A FE mesh composed of elements that are three-noded triangles was established, as depicted in Figure 2. The nodes correspond to the centroids of the blocks in the BM algorithm. The global displacement vector for each element, expressed in equation 7, contains the horizontal and vertical displacements for each node of the element. The design variables correspond to the set of global displacement vectors of all elements. They may also include the rotation angles of the blocks, leading to the rotational version of the algorithm; however, this information is not taken into account in the FE code.

$$\mathbf{b}_{\,element} = \begin{bmatrix} u_1 & v_1 & u_2 & v_2 & u_3 & v_3 \end{bmatrix} \tag{7}$$

Element interpolation functions ψ_i were then defined. In a FE methodology, the functions ψ_i allow the calculation of the horizontal $\mathbf{u}$ and vertical $\mathbf{v}$ displacements at each point (x, y) within the element by interpolation with the nodal displacements.

The strain distribution was computed within each element by multiplying the matrix of the shape function derivatives $\mathbf{B}$ by the global displacement

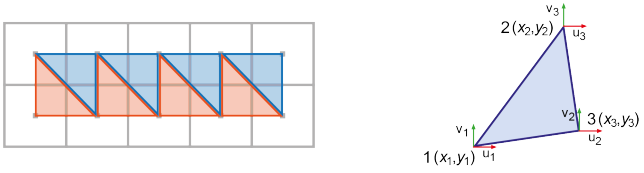

(a) (b)

Figure 2: On the left, the block mesh defined in grey. The centroids of the blocks constitute the nodes of linear triangular elements, in blue and orange. On the right, a linear triangular element composed of nodes 1, 2 and 3. To each node, a horizontal **u** and a vertical **v** displacement are assigned.

vector for that element:

$$\varepsilon = \begin{Bmatrix} \varepsilon_{11} \\ \varepsilon_{22} \\ 2\varepsilon_{12} \end{Bmatrix} = [\mathbf{B}]\,\mathbf{b}_{\,element} \tag{8}$$

For linear triangular elements, the matrix of the shape function derivatives **B** is constant, meaning that the deformation is also constant within each element. Strain is a dimensionless quantity representing deformation of a body. For each element, two normal strains, ε_{11}, ε_{22}, and a shear strain, $2\varepsilon_{12} = \gamma_{12}$, are obtained. The SE density can be calculated within each element by:

$$SED_{\,element} = \frac{1}{2}\varepsilon^{\,T}\sigma\varepsilon = \frac{1}{2}\varepsilon^{\,T}\,[\mathbf{D}]\,\varepsilon \tag{9}$$

By multiplying it by the area of the element, the total SE stored within the element is obtained:

$$SE_{\,element} = A_{\,element} \cdot U_{\,element} \tag{10}$$

Matrix **D** includes information regarding the Poisson's ratio ν of the solid's material, related to the deformation of a material in directions perpendicular to the direction of loading.

The total SE associated with a given configuration, equal to the E_R term in equation 5, is the sum of the SEs for all triangular elements. In practice, a relative SE is computed between two consecutive frames using a set of nodal displacements that are optimized from one frame to another.

2.4.2 Optimization strategy

Evolutionary algorithms, namely genetic algorithms (GAs) and particle swarm optimization (PSO), were selected to address the optimization strategy. These heuristic methods are suitable for solving motion estimation problems since they can have a greater capacity than traditional methods to deal with local minima and thus find the global minima under the conditions of an ill-posed problem [2]. The simulations were conducted on a hexacore Intel Core i7-8700 CPU with 64GB RAM. In MATLAB, parallel processing with six workers was applied to speed up the simulations.

The algorithm starts with a random collection of design variables (the population) that, through specific stochastic processes, is improved for each generation [2]. Preliminary experiments on the optimization strategy showed that the establishment of an initial population composed of 200 individuals and a stopping criterion of a maximum number of 150 iterations could guarantee a good convergence. Information concerning upper and lower bounds for the blocks' displacements and orientations was also provided to the optimizer, based on the values of the search window width p (defined as 5 for the synthetic images and as 7 or 15 according to the amplitude of motion in the echocardiographic images analysed) and on the most suitable search angle ranges for each image sequence studied. To speed up and facilitate the optimization strategy, initial estimates of the motion field at each frame for each image sequence, corresponding to the best five motion estimates, provided by the remaining BM algorithms, were inserted as individuals in the initial population.

For each set of parameters and a given image sequence, the algorithm was run 30 times to provide confidence to the results.

2.5. Validation

The validation and evaluation of the proposed BM approaches were done using synthetic image sequences for which the ground-truth solutions are known. The synthetic images were generated using FE models developed in *Abaqus* 2017 software. They corresponded to six distinct motions of a single beam when subjected to different loading and boundary conditions, namely two translational and one rotational rigid body motions, and uniform stretching, non-uniform stretching and bending. The beam model is 16.49 mm long and 3.74 mm high, similarly to the mitral valve leaflets' dimensions in the studied echocardiographic images. The FE mesh is composed of linear quadrangular elements whose approximate global size is 0.170 mm.

In MATLAB, figures representing the FE models estimated by *Abaqus* were created. At each step of each FE analysis, information regarding elements'

and nodal connectivities, as well the nodal coordinates and displacements, was extracted from *report* and *.rpy Abaqus* files and stored to create a figure corresponding to that step. This figure was processed so that the beam is presented in greyscale, considering a pixel depth of 8 bit. The images were saved in the *.png* format with a resolution of 0.170 mm and size 708 × 1016 pixels, just as the echocardiographic images studied. Each image sequence was composed of 11 frames. The filling of the beam using the greyscale in each frame was linear.

The synthetic images provided both a qualitative and quantitative assessment of the implemented algorithms. While the qualitative evaluation consisted only in visual inspection, the quantitative evaluation of the algorithms' performance was done by comparing the exact solutions provided by the FEMs for the displacement fields with those from the implemented algorithms. The FEM deformation estimates were computed analogously as in equation 8, using the nodal coordinates and displacements extracted from the FE analyses.

2.5.1 Evaluation metrics

The tracking error between an exact position $(x, y)_k$ and an estimated position $(\hat{x, y})_k$ was defined as:

$$e_k = \left\| (x, y)_k - (\hat{x, y})_k \right\|_2 \tag{11}$$

It thus provides the error amplitude between both positions. For each simulation of the algorithms, 100 positions corresponding to the centroids of 100 blocks, were initialized randomly in the first frame of each image sequence over the image region that corresponded to the beam. The tracking error was calculated for each one of these positions and averaged across all frames in the image sequence, considering all blocks simultaneously, then providing a global average tracking error (GATE). Note that a GATE of 0.170 mm is equivalent to a pixel. The standard deviation (SD), as well as the root-mean-square error (RMSE), were also computed using these ground-truth and estimated positions. When comparing strain values, the preferred metrics were absolute and relative errors.

Considering the different methodology of the optimization-based BM, a mesh of 30 non-overlapping blocks arranged in three rows was initialized over the beam in the synthetic image to allow the evaluation of this algorithm. The positions of the 100 random points initialized previously thus depended on the evolution of this block mesh.

The usage of large sample sizes or repetitions prompted for a statistical analysis of the results when studying each algorithm's performance using the synthetic images. The significance of measurements was evaluated by the Student's t-test; a paired analysis between two samples was performed and analysed comparing a confidence level of 0.95 to the *p-value*.

The real echocardiographic data studied consist of a 2D transesophageal echocardiography (TEE) image sequence of a mid-esophageal long-axis view acquired with the Vivid^{TM} E95 ultrasound equipment. It has a total of 181 frames acquired at a frame rate of 79 frames per second. Each pixel increment corresponds to 0.170 mm in both image directions. The performed analysis started during the end-diastole moment of the cardiac cycle, composed of 60 frames. No post-processing of the image sequence was performed. Over the two mitral leaflets, blocks of size n=10 arranged in two rows were initialized. The strain estimates were evaluated only visually since no ground-truth solution as available. Relevant geometrical quantities were derived from the tracking data semi-automatically.

3. Results and Discussion

3.1. Tracking results

3.1.1 Baseline solution

The baseline solution consisted of applying the *full search* algorithm. The impact of the block size n and p on the results was studied, as depicted in Figure 3.

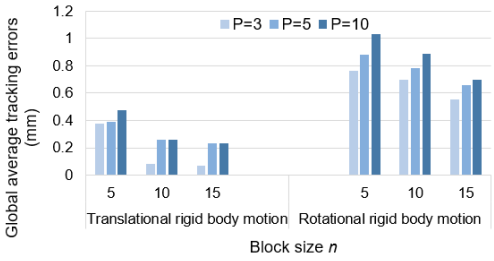

Figure 3: GATEs, in mm, provided by the baseline solution for two of the rigid body motions studied.

Overall, the more complex the motion, the greater the tracking error. The estimates were on average better if n was larger since it was more prone to capture distinct image features. For a fixed n, the best estimates were obtained for p=3, suggesting that the search window width should be adjusted as much as possible to the range of motion to ensure the best tracking. This arises as a need due to the ill-posedness of the motion tracking problem and to the fact that the SAD only encounters pixels' intensities in its evaluation, which may lead to the evaluation of infeasible matches if p is too large. For the bending case and n=10 (GATE=1.276 mm), a p=5 wasmore suitable given its broader MVs' amplitudes.

Larger errors were found to be associated mainly to blocks initialized in more homogeneous regions

of the body, in which the SAD was not sensitive enough to distinguish between similar blocks.

3.1.2 Rotational BM

The rotational BM aims to find a match with a lower SAD than the *full search* algorithm since it can adjust each block's orientation to the motion being tracked. Figure 4 presents the average SADs per block for different sets of tracking parameters. Regardless of the rotation parameters chosen, it decreased with the introduction of the rotational BM algorithm. The lowest SADs were obtained for the smallest search angle interval considered as it allowed the evaluation of a larger number of distinct orientations, less probably missing the best match.

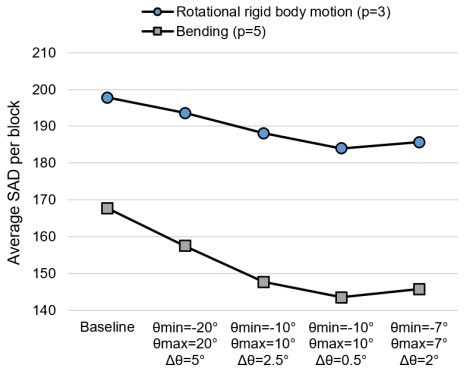

Figure 4: Average SAD per block obtained for the *full search* and rotational BM algorithms, for different sets of angle ranges, defined by θ_{min} and θ_{max}, and intervals $\Delta\theta$. A fixed block size n=10 was used.

The lowest average SADs were obtained for the bending case, suggesting that this approach was more suitable for tracking this motion. Indeed, when applied to this image sequence, a 26.1% reduction in the RMSE (for $\theta_{min} = -10°$, $\theta_{max} = 10°$ and $\Delta\theta = 2.5°$) compared to the baseline solution was reached. For the rotational rigid body motion, this algorithm did not appear to be as effective. Despite enhancing the baseline estimates for specific sets of parameters, only 1.31% reduction was verified (for $\theta_{min} = -7°$, $\theta_{max} = 7°$ and $\Delta\theta = 2°$) compared to the baseline solution.

3.1.3 Neighbourhood averaging

The neighbourhood averaging filtering (NAF) approach worked particularly well for the rotational rigid body motion. By fixing p=3 from the previous results, better enhancements were reached if information provided by all the eight neighbouring blocks was considered. It was effective for blocks of size n=5 that highly depend on neighbouring information to achieve a good tracking, but also worked particularly well for block sizes of n=10. The GATEs for n=10 and p=3 are depicted in Figure 5. The NAF has shown to have an especially positive impact on blocks located in regions of the beam where the baseline tracking estimate was poorer. Overall, the MVs appeared to be more regularized relatively to each other; however, some tracking errors still occurred in more homogeneous regions of the beam.

For the translation and bending cases, the NAF did not necessarily lead to enhanced tracking results. In the rotational rigid body motion, all particles in the beam are disposed linearly and present the same orientation relative to each other in each frame, which allowed the linear weighted averaging of the NAF approach to handle better this distribution. In the bending case, the NAF could not capture well the complex beam deflection and the differences in blocks' orientations while the rotational BM algorithm was.

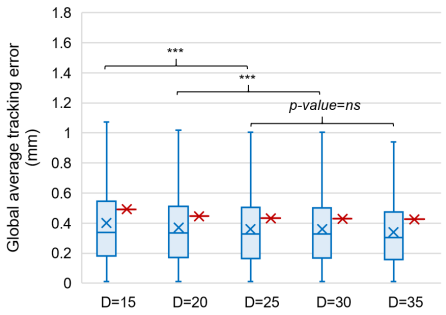

Figure 5: Box plots of the GATEs, in mm, for the rotational rigid body motion, after considering the NAF for different values of D and fixed n=10, p=3 and *type*=2 neighbours. The corresponding RMSE is marked in red on the right of each box.

When combining this approach with the rotational BM algorithm, analogous findings for each image sequence were obtained. The parameters that regulate the influence of the neighbouring information should be selected flexibly.

3.1.4 Optimization-based BM

Several aspects must be considered when studying the optimization-based BM algorithm. First of all, the overall performance of the GA and PSO algorithm was evaluated through the study of the rotational rigid body motion with a large regularization parameter λ=5000 for which the algorithm must converge to zero. The PSO algorithm was shown to be more effective and consistent for both versions of the optimization-based approach. In 30 simulations for each version of the optimization-based BM for this image sequence, the PSO lead, on average and considering all frames, always to lower cost function values. Results regarding the computational times

of each optimization strategy were not conclusive. As the consistency and efficiency of the method in finding the minimum was considered to be more important, the PSO algorithm was chosen to be used in the following simulations. It was also noted that the rotational version of the optimization-based BM algorithm took on average more 45 minutes than the translational one, which is a proof of its increased complexity given that there is a larger number of design variables to optimize.

The role of λ on the tracking results of the different image sequences was studied. Values of λ equal to 100, 500, 1000, 5000 and 10000 were evaluated and kept constant throughout the whole optimization process. Smaller values of λ allow more flexibility between the positions of blocks relative to each other, while larger values lead to more regularized motion fields, as they emphasize the regularization term versus the similarity term.

Distinct values of λ were found more suitable for different motion patterns. For the rotational rigid body motion, λs of 500 (GATE=0.302 mm) or 1000 (GATE=0.314 mm) were the most suitable choice. Both versions of the optimization-based BM led to similar results, which was expected since the rotation of blocks did not prove to be decisive in tracking this motion. The rotation of blocks was also not considered in the regularization term of the cost function, which can explain such results.

For the uniform and non-uniform stretching cases, λs of 5000 (GATE=0.312 mm) and 500 (GATE=0.164 mm) provided the lowest tracking errors, respectively. Both versions of the algorithm performed similarly as the motions are rectilinear.

The tracking errors for the bending case were significantly enhanced, attaining improvements of around 50% compared to the original baseline solution for λs of 500, 1000 and 5000 if the rotation was considered. The corresponding GATEs are presented in Table 1. Despite the MVs being more regularized in the first frames, the tracking errors still tended to propagate throughout the image sequence as depicted in Figure 6. However, this is still an encouraging outcome since bending better resembles the motion of the mitral leaflets [7]. The results associated with a λ of 1000 were then analysed in the following sections.

The choice of the most suitable λ appeared to depend both on the type of motion being studied and on the magnitude of the displacements and strains each motion presented. Overall, when comparing the tracking errors with those of similar strategies found in the literature [11, 3], the GATEs were found to be larger, about 1 or 2 pixels on average. Such differences are believed to be associated with the fact that the latter methods present a subpixel accuracy and that the regularization term in these algorithms penalizes inconsistencies directly in the displacement field rather than using a secondary measurement as the SE. Besides, the validation strategies and the characteristics of the images used to evaluate the proposed tracking methods in the literature, namely their resolution, may affect the comparison of the results.

Table 1: GATEs, in mm, for the bending case considering distinct values of λ and a fixed n=10.

	Translational optimization-based BM	Rotational optimization-based BM
λ=500	0.454	0.363
λ=1000	0.446	0.360
λ=5000	0.530	0.358

3.2. Deformation computation results

The estimates for every deformation component associated with the optimization-based BM algorithm for a fixed λ of 1000 were computed for each one of 36 triangular elements within the block mesh defined. For the uniform and non-uniform image sequences, the estimates provided by the translational optimization-based BM were considered, whereas for the rotational rigid body and bending cases, the estimates provided by the rotational optimization-based BM were analysed. As the algorithm was executed 30 times for each synthetic image sequence, the average positions of each block at each frame were computed.

Visually, if the tracking quality was satisfactory, the strain estimates were more correct from a qualitative point of view. Twenty elements were able to capture correctly ε_{11} and ε_{22} strains and only 4 elements captured correctly γ_{12} in the rotational rigid body motion. Regarding the uniform stretching, it was again only possible to depict the correct deformation pattern locally in regions closer to where the beam was fixed, in which no tracking errors occurred. This is thought to be a consequence of the effect of a large λ. Similar conclusions for the non-uniform stretching case can be drawn.

Even in regions in which, qualitatively, the estimates were good, the strains were not accurate from a quantitative point a view. A small tracking error can cause large errors in strain computation. Also, by looking at Figures 7 and 8 in which the estimated and real strains are plotted, it is possible to ascertain that the in the first frames the estimates varied roughly between -0.1 and 0.1. Note that a total of 360 points are plotted. The estimates depended on the initial distance between nodes. For instance, as the initial distancing between blocks was of 10 pixels in the first frame, if a single node moves by one pixel, strain varied between -0.1 and 0.1. On the other hand, such findings are related to the resolution of the displacement field. A resolu-

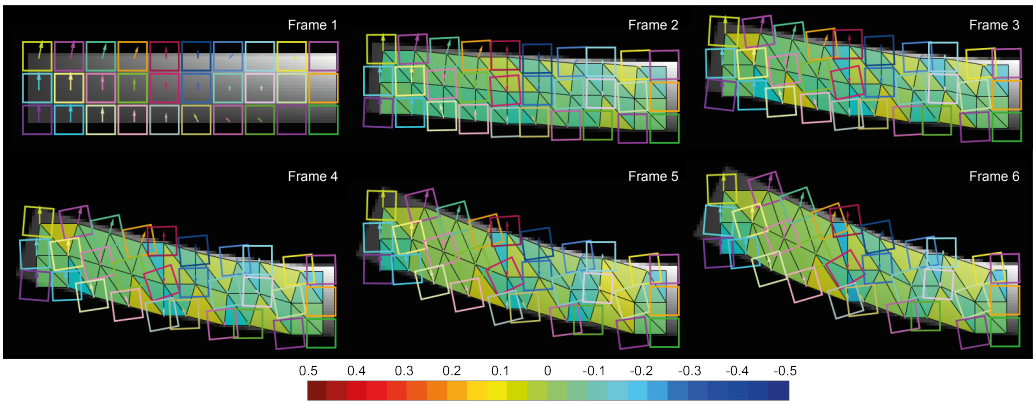

Figure 6: Motion tracking resulting from the application of the rotational version of the optimization-based BM to the bending image sequence, for λ=1000 and blocks of size n=10. The 30 non-overlapping blocks were initialized in frame 1 represent the different regions to be tracked. The arrows represent the different MVs when moving between two frames. The maximum absolute principal strains (a measure of strain intensity) are also illustrated according to a colour code presented on the bottom, being calculated between consecutive frames within each element.

tion of 1 pixel on the displacement's accuracy could not distinguish small deformations or, instead, led to rough strain estimates compared to the real ones. For instance, note how the strain estimates evolve in Figure 7 for the uniform stretching, a behaviour that is explained by such limitations. If a sub-pixel accuracy was simulated for this motion by performing a linear fit to the horizontal displacements of each node, the strain estimates would be improved, presenting only a relative error of 22.8%.

For the bending case, the results were considered to be favourable qualitatively if all points were placed in the first and third quadrants of the plots in Figure 8, representing the mechanical behaviour of the beam [5]. The majority of the scattered points that were not over the horizontal axis were indeed on these quadrants; when not, the erroneous strain estimates were associated with more notorious tracking errors. The estimates for the γ_{12} strains were not accurate from a quantitative or qualitative point of view since their computation involved more terms. Numerical inaccuracies such as inter-converting positions between pixels and mm may also affect these computations, especially if the strains' magnitudes are of the order of 10^{-3} or less.

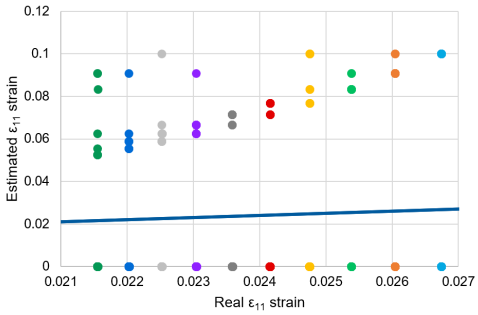

Figure 7: Correlation plot for the ε_{11} strain considering all elements and all frames for the uniform stretching case. Each different colour for the markers denotes a different pair of consecutive frames (from right to left, with the first pair in light blue on the right, and the tenth in darker green on the left). Points of the same colour should be overlapping and arranged along the straight line $\varepsilon_{estimated} = \varepsilon_{real}$ displayed in blue.

3.3. Real echocardiographic images results

The rotational version of the optimization-based BM algorithm, with λ=1000, appeared to be suitable when addressing the first frames of the TEE image sequence. During the end-closing and opening of the mitral valve, the algorithm could not capture the wider displacements of the mitral leaflets at their tips, not only due to their broader motion but also due to speckle decorrelation and poor image quality. A slight delay of the algorithm in detecting wider motions was identified. However, the MVs tried to follow the leaflets' motion, and the blocks maintained a relative positioning that resembles the leaflet's shape. To avoid the propagation of tracking errors throughout the image sequence, the algorithm was executed for only 20 frames (34 to 53) that comprise the different states of the mitral leaflets' positioning. Despite some improvements, some tracking errors still propagated, hampering the attainment of meaningful kinematic measurements. The motion tracking results are depicted in Figure 9.

Relevant geometrical parameters that could help distinguishing pathological conditions such as SMR

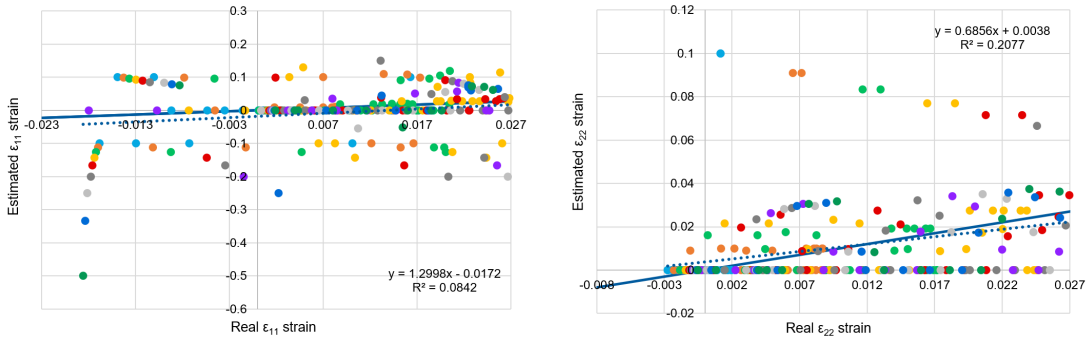

(a) ε_{11} strain

(b) ε_{22} strain

Figure 8: Correlation plots considering all elements and all frames for the bending case. Each different colour for the markers denotes a different pair of consecutive frames (in ascending order, respectively light blue, orange, light green, yellow, red, dark grey, purple, light grey, dark blue and dark green). Points should be arranged along the straight line $\varepsilon_{estimated} = \varepsilon_{real}$ displayed in blue. The dashed line represents the regression line that better fits such data, whose equation is reported inside the plot.

were studied [9]. The anteroposterior diameter was found to increase around 2.6% its diameter from end-systole to diastole, in agreement to what was found in the literature for healthy cases [9]. The anterolateral angle was indeed larger in diastole (179.91°) than in systole (159.86°). The bending distance was found to be 5.58 mm and 5.31 mm for the anterior and posterior leaflets respectively, suggesting that the valve opening is fairly symmetric. The coaptation distance was found to be 12.91 mm.

Qualitatively, closer to the annulus where the tracking was better, the anterior leaflet presented higher principal strains than the posterior leaflet. However, higher strain intensities are reported in the posterior leaflets in both normal in regurgitant valves [4]. Both stretching and compression were detected along the leaflets, given the dynamic nature of these structures. Despite the tracking impairments, in the first frames of the diastole phase (35 to 38) many elements of the posterior leaflet presented higher strain concentrations in the boundary zone near the annulus, as suggested in [4].

4. Conclusions

In this work, the performance of several BM approaches used in STE for the study of the mitral leaflets kinematics was assessed using synthetic generated images and a real TEE sequence.

The tracking results enhanced as the BM approaches increased their complexity. When an optimization-based BM algorithm was considered, they improved significantly for the complex bending case. Nevertheless, there were still tracking inaccuracies that precluded a correct estimation of the MVs and, consequently, of strains. Those were found to have a greater qualitative than quantitative value, being inaccurate mainly due to the lack of resolution in the displacement field, prompting for the attainment of tracking at sub-pixel accuracy.

The optimization-based BM algorithm had some difficulties in capturing motion correctly when the leaflets' displacements were wider in a TEE sequence. Due to speckle decorrelation noise, tracking errors propagated throughout the cardiac cycle, sometimes leading to a meaningless kinematic characterization of the leaflets. Distinct regularization functions and optimization strategies should be investigated to move towards deformable image registration approaches [15], proven to be competitive with other state-of-the-art STE algorithms.

5. Acknowledgments

This document was written and made publicly available as an institutional academic requirement and as a part of the evaluation of the MSc Thesis in Biomedical Engineering of the author at Instituto Superior Técnico. The work described herein was performed at Departamento de Engenharia Mecânica of Instituto Superior Técnico (Lisbon, Portugal), during the period September 2019-September 2020, under the supervision of Prof. João Folgado and Prof. Carlos Quental.

References

[1] M. S. Amzulescu, M. De Craene, H. Langet, A. Pasquet, D. Vancraeynest, A.-C. Pouleur, J.-L. Vanoverschelde, and B. Gerber. Myocardial strain imaging: review of general principles, validation, and sources of discrepancies. *European Heart Journal-Cardiovascular Imaging*, 2019.

[2] J. S. Arora. *Introduction to optimum design*. Elsevier, 2004.

[3] N. Azarmehr, X. Ye, J. D. Howes, B. Docking, J. P. Howard, D. P. Francis, and M. Zolgharni.

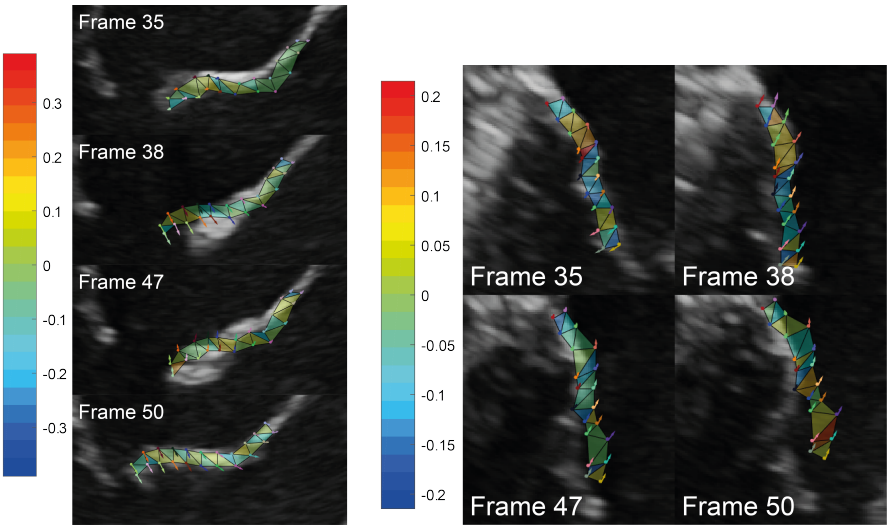

(a) Anterior leaflet. (b) Posterior leaflet.

Figure 9: Motion tracking resulting from applying the optimization-based BM algorithm on the mitral leaflets with λ=1000 to frames 44-53 of a cardiac cycle. The coloured dots represent the centroids of the blocks first initialized along the valve contour, while the arrows depict the corresponding MVs. The maximum absolute principal strains (a measure of strain intensity) are illustrated according to a colour code presented on the left, being computed between consecutive frames within each element.

An optimisation-based iterative approach for speckle tracking echocardiography. *Medical & Biological Engineering & Computing*, 2020.

[4] S. Ben Zekry, J. Freeman, A. Jajoo, J. He, S. H. Little, G. M. Lawrie, R. Azencott, and W. A. Zoghbi. Patient-specific quantitation of mitral valve strain by computer analysis of three-dimensional echocardiography: a pilot study. *Circulation: Cardiovascular Imaging*, 2016.

[5] A. F. Bower. *Applied mechanics of solids*. CRC press, 2009.

[6] Y.-K. Chen, Y.-T. Lin, and S.-Y. Kung. A feature tracking algorithm using neighborhood relaxation with multi-candidate pre-screening. In *Proceedings of 3rd IEEE International Conference on Image Processing*, 1996.

[7] K. Fattouch, P. Lancellotti, and G. D. Angelini. *Secondary Mitral Valve Regurgitation*. Springer, 1^{st} edition, 2015.

[8] D. Garcia, P. Lantelme, and E. Saloux. Introduction to speckle tracking in cardiac ultrasound imaging. *Handbook of Speckle Filtering and Tracking in Cardiovascular Ultrasound Imaging and Video. Institution of Engineering and Technology*, 2018.

[9] A. Hossien, P. Nithiarasu, E. Cheriex, J. Maessen, P. Sardari Nia, and S. Ashraf. A multidimensional dynamic quantification tool for the mitral valve. *Interactive cardiovascular and thoracic surgery*, 2015.

[10] B. Iung, G. Baron, E. G. Butchart, F. Delahaye, C. Gohlke-Bärwolf, O. W. Levang, P. Tornos, J.-L. Vanoverschelde, F. Vermeer, E. Boersma, et al. A prospective survey of patients with valvular heart disease in europe: The euro heart survey on valvular heart disease. *European heart journal*, 2003.

[11] H. Khamis, S. Shimoni, A. Hagendorff, N. Smirin, Z. Friedman, and D. Adam. Optimization-based speckle tracking algorithm for left ventricle strain estimation: A feasibility study. *IEEE transactions on ultrasonics, ferroelectrics, and frequency control*, 2016.

[12] P. Lancellotti, J. Zamorano, L. Badano, and G. Habib. *The EACVI textbook of echocardiography*. Oxford University Press, 2016.

[13] K.-H. Ng, L.-M. Po, K.-W. Cheung, and K.-M. Wong. Block-matching translational and rotational motion compensated prediction using interpolated reference frame. *EURASIP Journal on Advances in Signal Processing*, 2010.

[14] B. Pesquet-Popescu, M. Cagnazzo, and F. Dufaux. Motion estimation techniques. *Telecom ParisTech*, 2016.

[15] A. Sotiras, C. Davatzikos, and N. Paragios. Deformable medical image registration: A survey. *IEEE transactions on medical imaging*, 2013.